Corrosion Science 50 (2008) 2012–2020

Contents lists available at ScienceDirect

Corrosion Science

journal homepage: www.elsevier.com/locate/corsci

Photocurrent spectroscopy applied to the characterization of passive films on sputter-deposited Ti–Zr alloys

M. Santamaria [a,*], F. Di Quarto [a], H. Habazaki [b]

[a] Dipartimento di Ingegneria Chimica dei Processi e dei Materiali, Università di Palermo, Viale delle Scienze, 90128 Palermo, Italy
[b] Graduate School of Engineering, Hokkaido University, Sapporo 060-8628, Japan

ARTICLE INFO

Article history:
Received 29 January 2008
Accepted 23 April 2008
Available online 29 April 2008

Keywords:
A. Ti–Zr alloys
A. Passive film
B. Photocurrent spectroscopy
C. Band gap
C. Flat band potential

ABSTRACT

A photoelectrochemical investigation on thin (⩽13 nm) mixed oxides grown on sputter-deposited Ti–Zr alloys of different composition by air exposure and by anodizing (formation voltage, U_F = 4 V/SCE) was carried out. The experimental results showed that the optical band gap, E_g^{opt}, increases with increasing Zr content in both air formed and anodic films. Such behaviour is in agreement with the theoretical expectation based on the correlation between the band gap values of oxides and the difference of electronegativity of their constituents. The flat band potential of the mixed oxides was found to be almost independent on the Ti/Zr ratio into the film and more anodic with respect to those estimated for oxide grown on pure Zr. The semiconducting or insulating character of the investigated films was strongly influenced by the forming conditions and the alloy composition.

1. Introduction

In the last years Ti and Zr containing mixed oxides have attracted the attention of several research groups due to their applications in a wide range of technological fields. For instance, chemical vapour deposited $Zr_{0.65}Ti_{0.35}O_2$ thin films [1] are promising candidate for gate-dielectric applications, since their use is reported to improve the scalability and to reduce the leakage current of complementary metal-oxide-semiconductor (CMOS) transistors. Moreover, sol–gel prepared Ti–Zr mixed oxides of several compositions seem to improve the efficiency of dye-sensitized solar cells with respect to those fabricated with pure TiO_2 [2–4] and show enhanced photocatalytic activity for photovoltaic oxidation of organic pollutants compared to pure TiO_2 [5–7]. Due to their high thermal stability, TiO_2–ZrO_2 mixed oxides prepared by precipitation from homogenous solution have also been tested to be very good catalyst support [8]. Finally, alloying addition of Zr to Ti metal allows the formation of passive films with higher corrosion resistance with respect to passive films on pure titanium [9–10].

For any of the listed applications the knowledge of mixed oxide solid state properties such as band gap, flat band potential and conduction type is a key factor for understanding their behaviour and improving their performance. In this work we report on a photoelectrochemical investigation on Ti–Zr mixed oxides, grown by air exposure and by anodizing at room temperature on sputter-deposited Ti–Zr alloys of different composition. The band gap values and the flat band potential of the investigated oxides are estimated as a function of the base alloy composition and of the forming conditions. The influence of Ti/Zr ratio on the insulating or semiconducting behaviour of the oxide is discussed.

2. Experimental

Zr–Ti alloy films, together with zirconium, were prepared by dc magnetron sputtering. Targets consisted of a 99.9% zirconium disk, of 100 mm diameter, with an appropriate number of 99.9% titanium disks, of 20 mm diameter, located symmetrically on the erosion region for preparation of the alloys. Substrates were glass plates. In order to obtain alloy films of uniform thickness and composition, the substrate holders were rotated around the central axis of the chamber, as well as about their own axes, during sputter deposition. As previously reported [11–12], all the deposited films were hcp solid solutions, whose compositions were determined by Rutherford backscattering spectroscopy.

Anodizing was undertaken in 0.1 M ammonium pentaborate (ABE) and 0.5 M H_2SO_4 electrolytes at 298 K potentiodynamically at 20 mV s^{-1}. A saturated calomel electrode (SCE) was employed as reference electrode. The experimental set-up employed for the photoelectrochemical investigations is described elsewhere [13]: it consists of a 450 W UV–VIS xenon lamp coupled with a monochromator (Kratos), which allows monochromatic irradiation of the specimen surface through the electrochemical cell quartz windows. A two-phase lock-in amplifier (EG&G) was used in connection with a mechanical chopper (frequency: 13 Hz) in order to separate the photocurrent from the total current circulating in

* Corresponding author. Tel.: +39 091 6567287; fax: +39 091 6567280.
E-mail address: santamaria@dicpm.unipa.it (M. Santamaria).

0010-938X/$ - see front matter © 2008 Elsevier Ltd. All rights reserved.
doi:10.1016/j.corsci.2008.04.014

the cell due to the potentiostatic control. Photocurrent spectra reported below are corrected for the relative photon flux of the light source at each wavelength, so that the photocurrent yield in arbitrary current units is represented in the *Y* axis.

All the experiments were performed in air at room temperature.

3. Results

3.1. Air formed films

After immersion of the Ti–Zr alloys in both 0.1 M ABE and 0.5 M H_2SO_4 solutions, the open circuit potentials, U_{OC}, of Table 1 were measured, with the most cathodic values pertaining to Zr and Zr rich alloys. In order to get some information on the nature of the initial air formed films on the alloys, a photoelectrochemical investigation has been performed at polarizing voltage, U_E, around U_{OC}. A very narrow ($U_E \leqslant 0.3$ V/SCE) potential range was exploited so that it was possible to assume that the polarization does not affect the nature and properties of the air formed films. The initial films were all photoactive at U_{OC} in both 0.1 M ABE and 0.5 M H_2SO_4 solutions with the presence of anodic photocurrent for all the investigated composition. This finding was assumed as an indication that the initial passive films present on these alloys consist of mixed oxide phases having a n-type semiconducting or insulating behaviour and flat band potentials slightly more negative than the initial U_{OC} value.

In Fig. 1a we report the photocurrent spectrum relating to an air formed film on Ti–42 at.%Zr, recorded by polarizing the electrode at U_{OC}. By assuming indirect optical transitions (see Fig. 1b) it was possible to derive the optical band gap value of the investigated films according to the following equation [13]:

$$(I_{ph}h\nu)^{0.5} \propto (h\nu - E_g^{opt}) \quad (1)$$

where, for photon energy in the vicinity of band gap, the photocurrent yield, I_{ph}, is proportional to the light absorption coefficient, $h\nu$ is the photon energy and E_g^{opt} is the optical band gap, or the mobility gap in the case of amorphous materials.

For all the investigated films an exponential decrease in the photocurrent yield (Urbach tail) as a function of photon energy was observed at photon energies lower than the mobility gap (part A of Fig. 1c). As already found for several anodic films on valve metals and valve metal alloys [13–16], a possible origin of such dependence is the variation of the light absorption coefficient according to the following law:

$$\alpha = \alpha_0 \exp\left(-\frac{E_0 - h\nu}{E_U}\right) \quad (2)$$

where α_0 is a constant and E_U is a measure of the width of band tails, i.e. the extent of DOS localization near the band edge. This relationship has been rationalized in the case of a-SCs by assuming an exponential distribution of localized states in the band edge tails [17]. In this cases E_0 marks the energy where $\ln\alpha$ vs $h\nu$ (Urbach plot) ceases to be linear and its value frequently coincides with the mobility gap of the material. For all the investigated air formed films, E_0 slightly higher than the mobility gap calculated according to Eq. (1) was determined (see Fig. 1b and c). At very low absorption levels, a second exponential part in the Urbach plot (weak absorption tail, B in Fig. 1c) was frequently observed. Such a behaviour has been interpreted by assuming a dependence of the light absorption coefficient on energy according to the following relationship:

$$\alpha \propto \exp\left(\frac{h\nu}{E_t}\right) \quad (3)$$

where the energy parameter E_t is always larger than E_U [18]. According to Ref. [18], this part of the $\log\alpha$ vs $h\nu$ plot is not as well reproducible as part A due the high structure sensitivity of the light absorption coefficient in this energy range.

In Table 1, we summarize the estimated band gap values of air formed films as a function of the base alloy composition. It is important to stress the following aspects: (1) no appreciable influence of the polarizing electrolyte has been evidenced in spite of the large difference of their pH; (2) E_g^{opt} increases as the Zr content in the base alloy increases; (3) in the photocurrent spectra relating to air formed films on Ti–80 at.%Zr a photocurrent tail was present at energy lower than the estimated band gap (see Fig. 2a), while for air formed films on Zr two linear regions were present in the $(I_{ph}h\nu)^{0.5}$ vs $h\nu$ plot, giving two possible extrapolated band gap values: E_{g1}^{opt} = 3.5 eV and E_{g2}^{opt} = 4.3 eV by fitting the low and high energy region, respectively (see Fig. 2b).

In order to get some information on the semiconducting or insulating character of the air formed films, we recorded photocurrent vs polarizing voltage curves (photocharacteristics) by scanning the electrode potential in the cathodic direction at 5 mV s^{-1} at constant irradiating wavelength. No inversion of the photocurrent sign was revealed for air formed films on Ti–Zr alloys with a zirconium content $\leqslant$63 at.% as typical of n-type semiconductors (see Fig. 3a). For these layers at all the investigated wavelengths the potential at which the photocurrent goes to zero in 0.1 M ABE is −0.8 ± 0.1 V(SCE), thus we can roughly locate the flat band potential around this value. A clear inversion of the photocurrent sign was present for air formed films on Ti–80 at.%Zr, as confirmed by the rapid change in the photocurrent phase angle, indicating an insulating behaviour of the film (see Fig. 3b). An inversion potential of −0.8 V(SCE) can be estimated from the photocharacteristics recorded in 0.1 M ABE at 240 nm and 280 nm. The onset of cathodic current hinders to get the inversion photocurrent potential for air formed films on pure Zr polarized in both 0.1 M ABE and 0.5 M H_2SO_4 electrolytes.

3.2. Anodic films

Anodic films on Zr–Ti alloys were grown to 4 V(SCE) at 20 mV s^{-1} in both 0.1 M ABE and 0.5 M H_2SO_4. From the anodizing ratios (i.e. the reciprocal of the electric filed during the film growth) estimated from data reported in Refs. [11–12], it is possible to calculate approximately a film thickness between 10 nm and 13 nm for the anodized alloys. All the films were photoactive and in Table 2 we report the indirect optical band gap values, measured by polarizing the oxides at 2 V(SCE), as shown in Fig. 4a and b for Ti–42 at.%Zr anodized to 4 V(SCE) in 0.1 M ABE. As already found for air formed films, the band gap values increases as the Zr content in the base alloys increases, even if anodic films have slightly lower band gap values with respect to air formed films grown on the alloy with the same composition. No appreciable influence of the anodizing electrolyte on E_g^{opt} values is observed.

It is interesting to stress that in the case of anodic films of 4 V(SCE) the photocurrent measured at very low energy (part B of Urbach plot) disappeared, also in the case of very pronounced

Table 1
Optical band gap values relating to air formed films on sputter-deposited Ti–Zr alloys, estimated by assuming non direct optical transitions

Base alloy	Sol: 0.1 M ABE		Sol: 0.5 M H_2SO_4	
	U_{OC} (V(SCE))	E_g^{opt} (eV)	U_{OC} (V(SCE))	E_g^{opt} (eV)
Ti–10 at.%Zr	−0.20	3.51	0.29	3.55
Ti–23 at.%Zr	−0.20	3.59	0.12	3.64
Ti–42 at.%Zr	−0.30	3.95	0.05	3.92
Ti–63 at.%Zr	−0.30	4.15	0.12	4.10
Ti–80 at.%Zr	−0.41	4.18	0.02	4.15
Zr	−0.55	3.50/4.30	− 0.21	3.50/4.30

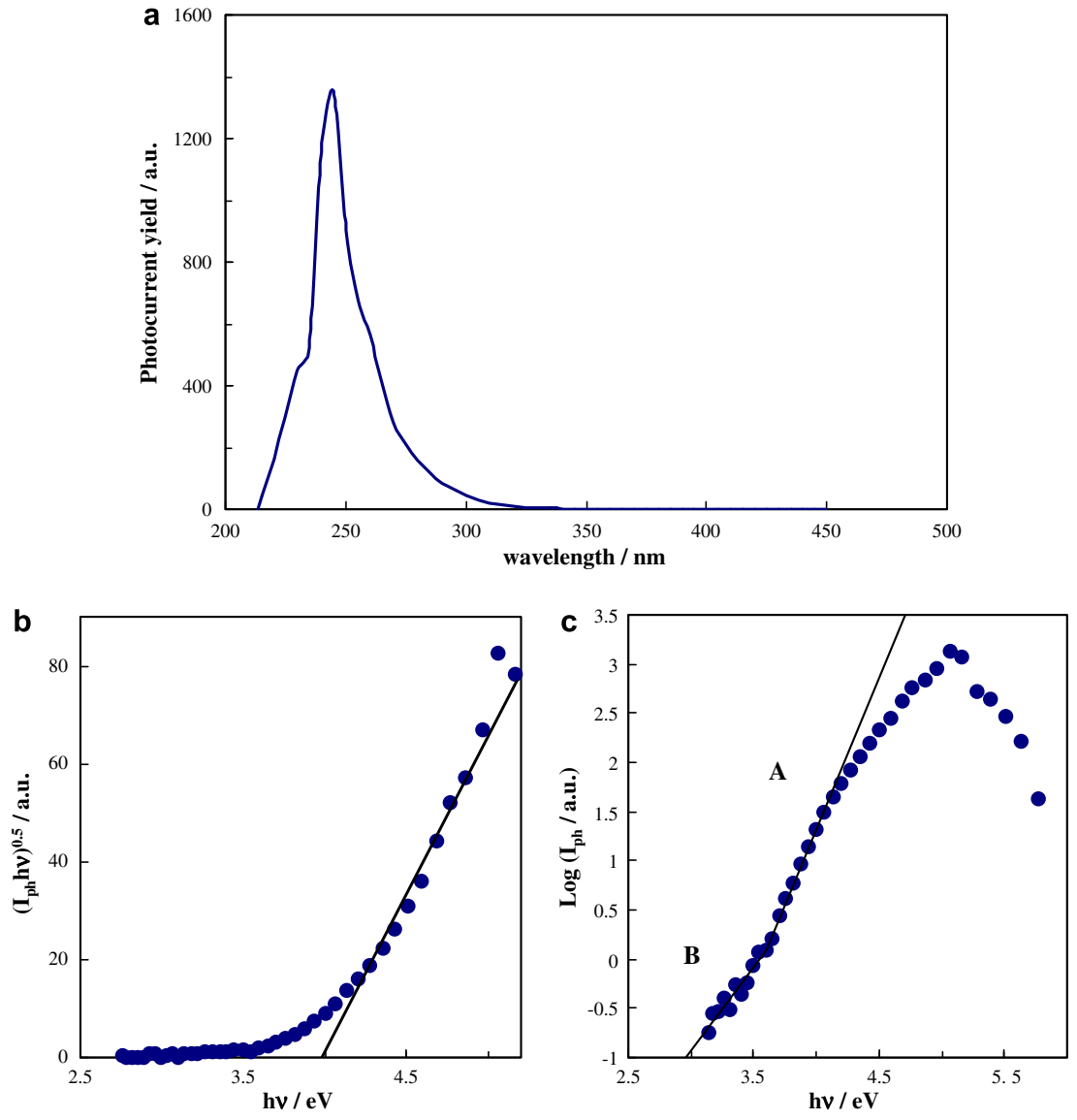

Fig. 1. (a) Photocurrent spectrum relating to air formed film on Ti–42 at.%Zr, recorded by polarizing the electrode in 0.1 M ABE at $U_E = U_{OC} = -0.30$ V(SCE). (b) $(I_{ph}h\nu)^{0.5}$ vs $h\nu$ and (c) Urbach plot.

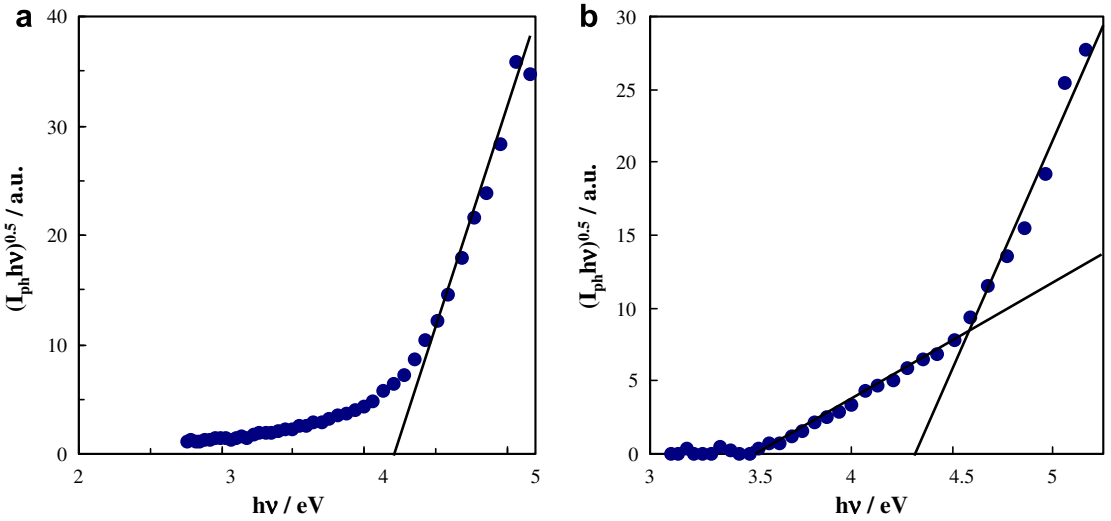

Fig. 2. $(I_{ph}h\nu)^{0.5}$ vs $h\nu$ plots relating to air formed film on (a) Ti–80 at.%Zr and (b) Zr, recorded in 0.1 M ABE at $U_E = -0.3$ V(SCE).

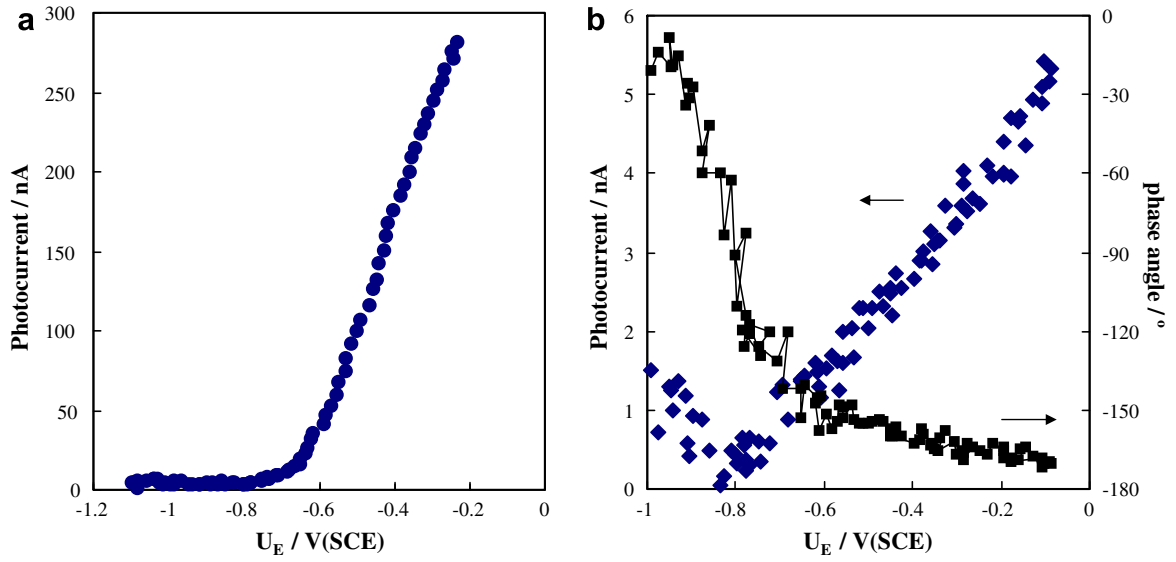

Fig. 3. (a) Photocurrent vs polarizing voltage curves for air formed film on Ti–23 at.%Zr. (b) Photocurrent and photocurrent phase angle vs polarizing voltage for air formed film on Ti–80 at.%Zr. Sol: 0.1 M ABE, λ = 280 nm and v_{scan} = 5 mV s^{-1}.

Table 2
Optical band gap values relating to anodic films grown to 4 V(SCE) at 20 mV s^{-1} on sputter-deposited Ti–Zr alloys, estimated by assuming non direct optical transitions at U_E = 2 V(SCE)

Base alloy	Sol: 0.1 M ABE E_g^{opt} (eV)	Sol: 0.5 M H_2SO_4 E_g^{opt} (eV)
Ti–10 at.%Zr	3.38	3.40
Ti–23 at.%Zr	3.48	3.47
Ti–42 at.%Zr	3.75	3.77
Ti–63 at.%Zr	4.0	4.0
Ti–80 at.%Zr	4.15	4.17
Zr	3.40/4.50	3.40/4.50

tailing as that evidenced for air formed film on Ti–80 at.%Zr (sse Fig. 2a). For 4 V(SCE) anodic films on Zr it is still possible to get two optical band gap values at high (4.5 ± 0.05 eV, see Table 2) and low photon energies (3.45 ± 0.05 eV, see Table 2). The origin of the sub-band gap photocurrent in anodic films on sputter-deposited Zr has been extensively discussed in Ref. [19] and it has been attributed to optical transitions involving a band of localized states inside the mobility gap of the film.

As found for the air formed films, an exponential decrease in the photocurrent yield as a function of photon energy has been observed at photon energies lower than the mobility gap for all the investigated anodic films (see Fig. 4c) with E_U values lower with respect to those estimated for the corresponding air formed films and increasing with increasing the Zr content in the base alloy (see Fig. 5). Therefore, the width of the band tail increases with increasing Zr content in the mixed oxides and decreases as the film thickness increases.

For anodized Ti–10 at.%Zr only anodic photocurrents were observed, as typical of n-type semiconducting materials and reminiscent of the behaviour of TiO_2, while both anodic and cathodic photocurrents were measured for anodized Ti–23 at.%Zr, in contrast with the behaviour of the air formed film on the same alloy. Thus, in spite of the low Zr content in the base alloy the anodizing process leads to the formation of an insulating layer. As expected, all the mixed oxide grown on Zr richer alloys both in slightly alkaline and acidic electrolytes behave like insulating materials with a clear inversion of the photocurrent sign in the photocharacteristics (see Fig. 6). The shape of the cathodic photocurrent spectra was quite similar to the corresponding anodic ones, allowing to estimate band gap values similar to those obtained from the anodic spectra (see Fig. 7).

4. Discussion

Previous work [20] proposed that the optical band gaps of crystalline oxides, M_xO_y, are proportional to the square of the electronegativity difference of their constituents, $(\chi_M - \chi_O)^2$, based on the assumption of a direct relation between the band gap and the single M—O bond energy, obtained from the Pauling equation for the single bond energy. The following equation was suggested to apply [13–15] to amorphous d metal oxides:

$$\text{d) } E_g^{opt} - \Delta E_{am}\ (\text{eV}) = 1.35(\chi_M - \chi_O)^2 - 1.49 \quad (4)$$

where ΔE_{am} is a parameter which takes into account the influence of amorphous nature on the band gap of the oxides. ΔE_{am} is zero for crystalline oxides, whilst increasing values are expected (up to around 0.5 eV) if the lattice disorder affects the density of states distribution near both the valence and conduction band edges [21].

For mixed oxides $A_aB_bO_y$, the previous correlation is still valid provided that the average single bond energy is estimated taking into account the contributions of both, A and B, cations of the oxide through an average cationic electronegativity parameter, χ_M, given by

$$\chi_M = x_a\chi_A + x_b\chi_B \quad (5)$$

where A and B are the metal cations in the oxide, and $x_{a,b}$ their cationic fractions. In order to use Eqs. (4) and (5) to fit the experimental band gap values of the investigated Ti–Zr mixed oxides, we assume x_{Zr} = 1.40 according to the Pauling scale, and χ_{Ti} = 1.656, obtained as the arithmetic mean between the electronegativity, calculated through Eq. (4) and by assuming 3.05 eV and 3.2 eV for the band gap values of rutile and anatase crystalline films [16]. This value is in the range of uncertainty estimated by Pauling. In Fig. 8 we compared the experimental E_g^{opt} values with the theoretical expectation (continuos line) for air formed and anodic films on the investigated Ti–Zr alloys (see Tables 1 and 2). It is important to stress that the Ti/Zr ratio in the films is assumed equal to that of the base alloys, in agreement with the compositional depth profiles reported

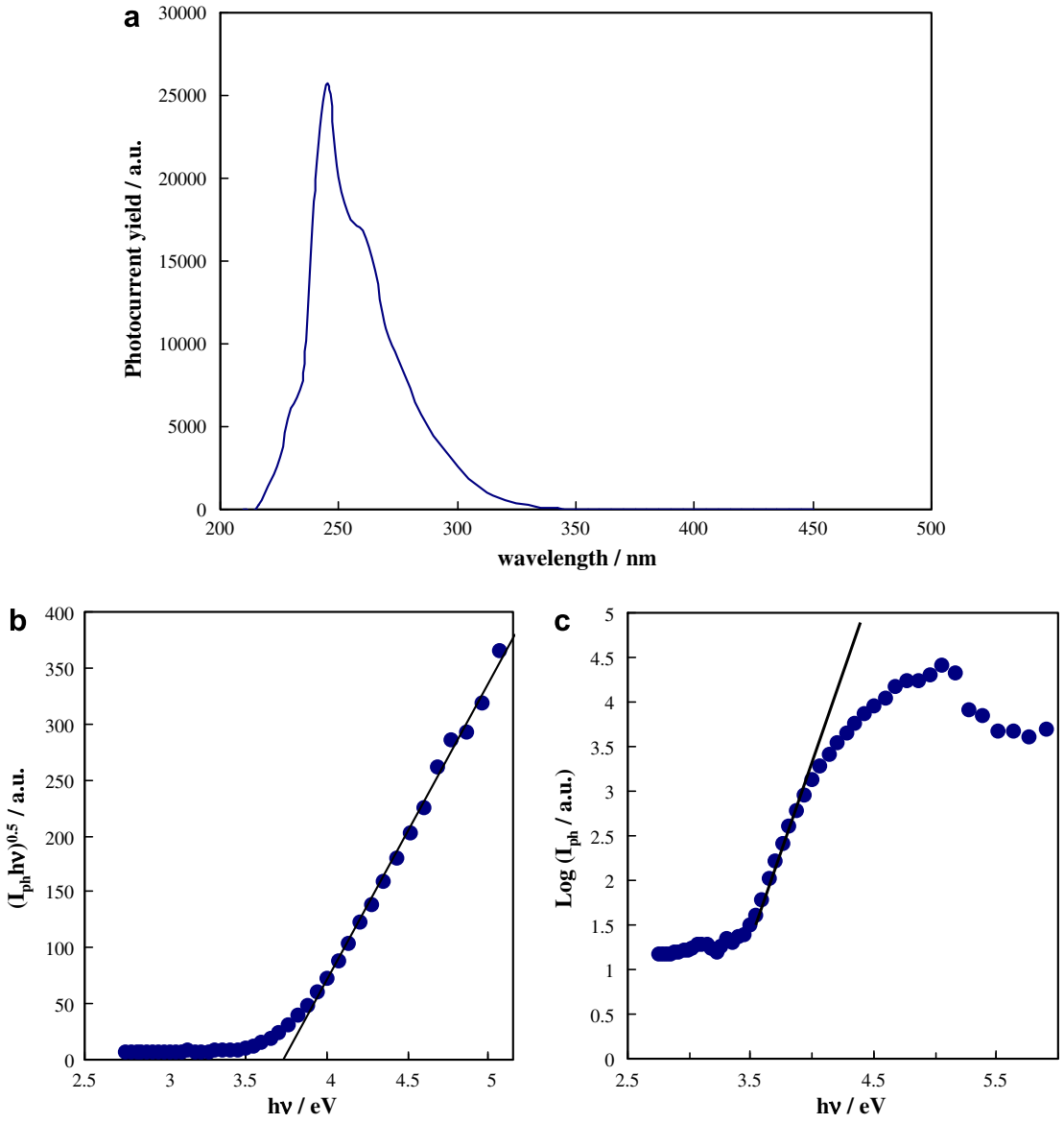

Fig. 4. (a) Photocurrent spectrum relating to an anodic film grown to 4 V(SCE) at 20 mV s^{-1} on Ti–42 at.%Zr, recorded by polarizing the electrode in 0.1 M ABE at U_E = 2 V(SCE). (b) $(I_{ph}h\nu)^{0.5}$ vs $h\nu$ and (c) Urbach plots.

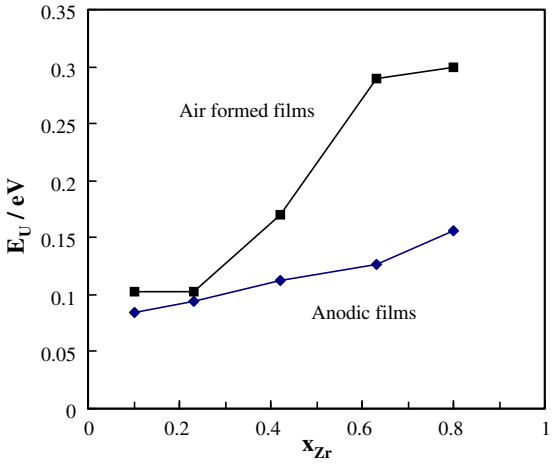

Fig. 5. E_U from the part A of the Urbach plots relating to air formed and anodic (U_F = 4 V/SCE) films on sputter-deposited Ti–Zr alloys recorded in 0.1 M ABE.

in Refs. [11–12], obtained by Rutherford back scattering and/or glow discharge optical emission spectroscopy for anodic films grown in ABE up to high formation voltages on Ti–Zr alloys, sputter-deposited in the same conditions.

As Fig. 8a shows, in the case of air formed films the experimental E_g^{opt} differs from the values calculated by means of Eqs. (4) and (5), by a quantity which is in the range foreseen by the taking into account the possible amorphous nature of the investigated layers. It is interesting to mention that: (1) the ΔE_{am} values estimated for air formed films are higher than those obtained for the corresponding anodic oxides (see Fig. 8a and b), suggesting a decrease in the lattice disorder of the film due to the anodizing process; (2) ΔE_{am} values decreasing with increasing Zr content in the mixed oxides were estimated, with $\Delta E_{am} \cong 0$ for the air formed and anodic films on Ti–80 at.%Zr. The dependence of ΔE_{am} on the film composition is in agreement with the GIXRD analysis reported in Ref. [12], where thicker anodic oxides on such alloys are reported to be amorphous for a zirconium content $\leqslant$42 at.%, microcrystalline and crystalline in the case of 63 at.%Zr and 80 at.%Zr, respectively.

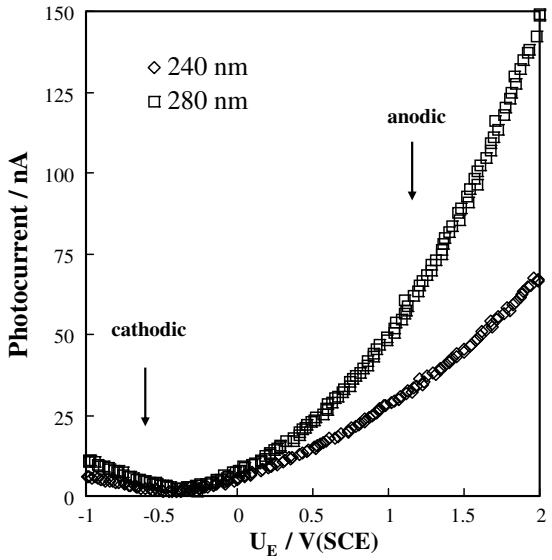

Fig. 6. Photocurrent vs polarizing voltage curves relating to anodic film (U_F = 4 V/SCE) on Ti–80 at.%Zr. Sol: 0.1 M ABE and v_{scan} = 5 mV s^{-1}.

In order to estimate the flat band potential of the anodic oxides the photocharacteristics were fitted according to a power law, $(I_{ph})^n \propto U_E$ (see Fig. 9), and a U_{FB} coincident with the extrapolated potential of zero photocurrent, V^*, was assumed [13–14]. The values of n and V^* obtained at each wavelength are reported in Table 3. The disclosed supralinear behaviour ($1/n > 1$) in a large potential range, as well as the dependence of n on the wavelength are attributed to the presence of initial (geminate) recombination effects of injected photocarriers, which are more pronounced in the case of anodic films on Zr rich alloys. Geminate recombination can occur if the thermalization length of the photogenerated electron–hole pairs is too short to prevent recombination of injected photocarriers. Such phenomenon is typical of low mobility carriers in crystalline materials and in amorphous materials containing a non zero density of localized states near the Fermi energy level [13–14]. Thus, the very low best fitting exponent estimated for anodic films on Zr rich alloys are in agreement with a wide region of localized states near the mobility edges, as suggested also by the Urbach plot. The influence of surface recombination phenomena on the I_{ph} vs U_E curves has been neglected due to the high electric field across the films in the fitted electrode potential region [13].

According to the data reported in Table 3, the V^* values are not appreciably dependent on the oxide composition. In fact, by averaging the zero photocurrent potentials estimated for all the investigated alloys a value of 0 ± 0.1 V(SCE) and a value of -0.55 ± 0.1 V(SCE) can be calculated from the photocharacteristics recorded in 0.5 M H_2SO_4 and 0.1 M ABE electrolytes, respectively, regardless of the alloy composition. The more anodic values estimated for films formed and characterized in 0.5 M H_2SO_4 electrolytes reported in Table 3, are in fair good agreement with the theory, which predicts a dependence of U_{FB} on the pH according to the relationship [22]:

$$U_{FB} = \text{const.} - 0.059\ \text{pH} \quad (6)$$

The V^* values measured for 4 V (SCE) mixed oxides are more anodic with respect to the extrapolated zero photocurrent potential measured for anodic films on Zr and almost coincident with the V^* values determined for anodic films grow on cast titanium [16]. If we take into account that the flat band potential of an insulating or semiconducting material is related to its Fermi level, E_F, by the following equation:

$$E_F = -|e|U_{FB} + |e|U_{+ref} \quad (7)$$

where e is the electron charge and U_{ref} is the potential of the employed reference electrode with respect to the vacuum scale, the almost independence of U_{FB} on oxide film composition and the widening of the band gap value with increasing Zr content in the oxide can explain the change from a n-type conductivity to an insulating behaviour with increasing the zirconium content in the film. In Fig. 10 we report a schematic picture of the variation of the band gap on going from the anodic film on Ti–10 at.%Zr to the anodic film on pure Zr. The energy levels are represented at pH 5.85, which is between the pH of zero charge reported for TiO_2 (5.8, according to Ref. [23]) and the pH of zero charge reported for ZrO_2 (5.9, according to Ref. [23]).

As for the energy levels location relating to the anodic oxide on Ti–10 at.%Zr, the conduction band mobility edge, E_C, is assumed ~0.4 eV above the E_F, by analogy with $(E_C - E_F)$ values reported for amorphous anodic films on titanium [24], thus allowing to locate the valence band mobility edge, E_V, from the calculated optical

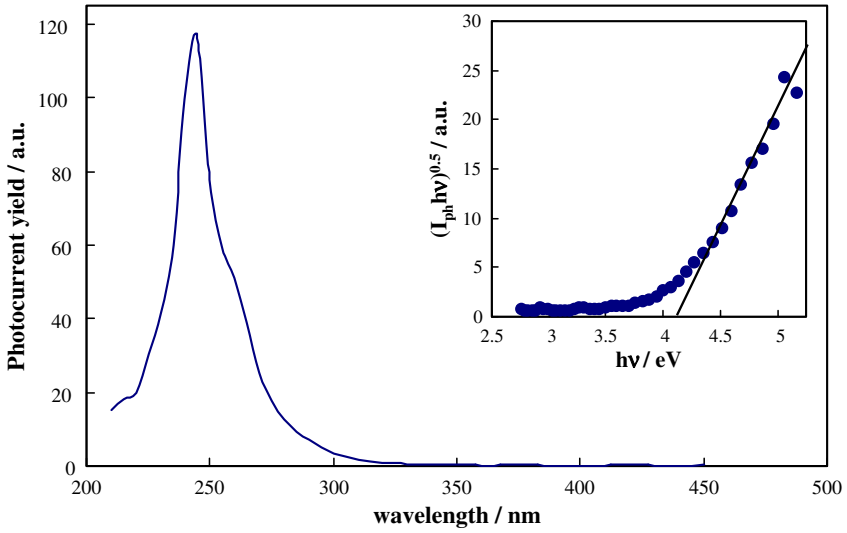

Fig. 7. Photocurrent spectrum relating to an anodic film grown to 4 V(SCE) at 20 mV s^{-1} on Ti–63 at.%Zr, recorded by polarizing the electrode in 0.1 M ABE at $U_E = -1.1$ V(SCE). Inset: $(I_{ph}h\nu)^{0.5}$ vs $h\nu$ plot.

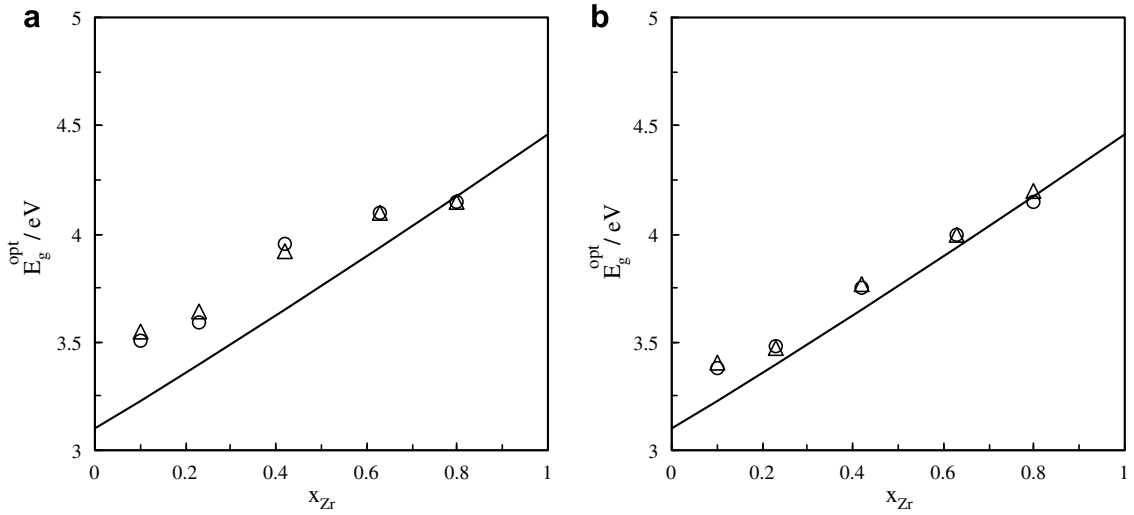

Fig. 8. Optical band gap as a function of the Zr cationic fraction for (a) air formed and (b) anodic films (U_F = 4 V/SCE) Ti–Zr alloys. Polarizing electrolyte: 0.1 M ABE (○) and 0.5 M H_2SO_4 (△). Continuos line represents the expected E_g^{opt} from Eqs. (4) and (5).

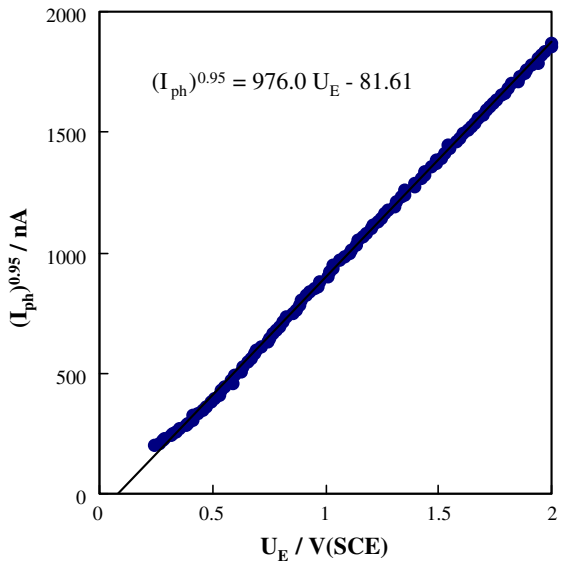

Fig. 9. Fitting of the I_{ph} vs polarizing voltage curve relating to an anodic film grown to 4 V(SCE) at 20 mV s^{-1} on Ti–10 at.%Zr. Sol: 0.5 M H_2SO_4, λ = 280 nm and v_{scan} = 5 mV s^{-1}.

band gap. Concerning anodic ZrO_2, E_C is located 1.8 eV above the zirconium metal Fermi level (−4 eV), according to the Fowler threshold energy estimated for anodic films on sputter-deposited Zr of different thickness [19]. From the energetics depicted in Fig. 10 it is evident that the band gap widening with increasing Zr content is mainly sustained by the shift toward higher energy of the conduction band edge. This is expected since the valence band is constituted by the O 2p orbitals of the oxides, while the conduction band is constituted predominantly by the Ti 3d and Zr 4d orbitals on going from Ti rich to Zr rich oxides. The almost constancy of the mixed oxides Fermi level and the simultaneous variation of the band gap value cause an increasing energy distance between E_C and E_F, which can explain the change from a n-type semiconducting behaviour to an insulating behaviour by increasing Zr content.

Moreover, it is interesting to mention that the flat band potential of the air formed films is more cathodic with respect to the corresponding anodic layers. The flat band potential of an oxide is

Table 3a
Parameters obtained by fitting according to power law $(I_{ph})^n \propto (U_E - V^*)$ the experimental photocharacteristics recorded for anodic films grown to 4 V(SCE) at 20 mV s^{-1} on sputter-deposited Ti–Zr alloys in 0.5 M H_2SO_4

Base alloy	λ (nm)	n	V^* (V(SCE))
Ti–10 at.%Zr	240	0.95	0.04
	280	0.90	0.08
	320	0.825	0.03
	360	0.725	−0.07
Ti–23 at.%Zr	240	0.90	0.07
	280	0.65	0.06
	320	0.55	0.01
Ti–42 at.%Zr	240	0.70	−0.02
	280	0.575	−0.03
	320	0.50	−0.02
Ti–63 at.%Zr	240	0.65	0.06
	280	0.55	0.08
Ti–80 at.%Zr	240	0.625	−0.02
	280	0.55	−0.09
Zr	240	0.825	−0.74

Table 3b
Parameters obtained by fitting according to power law $(I_{ph})^n \propto (U_E - V^*)$ the experimental photocharacteristics recorded for anodic films grown to 4 V(SCE) at 20 mV s^{-1} on sputter-deposited Ti–Zr alloys in 0.1 M ABE

Base alloy	λ (nm)	n	V^* (V(SCE))
Ti–10 at.%Zr	240	0.95	−0.45
	280	0.70	−0.49
	320	0.60	−0.46
	360	0.575	−0.49
Ti–23 at.%Zr	240	0.90	−0.45
	280	0.65	−0.52
	320	0.575	−0.48
Ti–42 at.%Zr	240	0.70	−0.55
	280	0.525	−0.57
	320	0.475	−0.56
Ti–63 at.%Zr	240	0.65	−0.55
	280	0.50	−0.67
Ti–80 at.%Zr	240	0.60	−0.54
	280	0.50	−0.57
Zr	240	0.75	−1.23

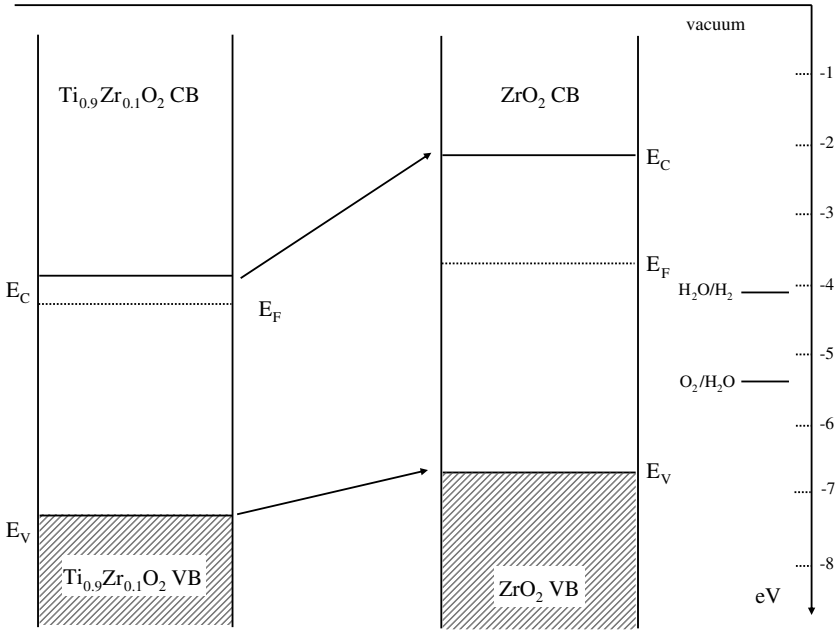

Fig. 10. Schematic picture of the variation of the band gap on going from anodic film on Ti–10 at.%Zr to anodic film on pure Zr.

dependent on the doping concentration as well as on the density of states within the mobility gap. In both crystalline and amorphous materials the presence of imperfections, like impurities, dangling bond at point defects, microvoids, non stoichiometry etc., can originate such kind of localized levels. The formation of an oxygen deficient phase is reported to occur for both TiO_2 [25] and ZrO_2 ([19] and references therein). In the first case the presence of oxygen vacancies is considered responsible of the n-type conductivity of titanium oxide. Thus, we can assume that a non stoichiometry due to an oxygen deficiency is also present in the Ti–Zr containing mixed oxides, in agreement with what suggested in Ref. [5] for crystalline $TiZrO_4$. The Fermi level position is determined by the interplay between the density of state inside the mobility gap (decreasing with increasing crystallinity) and the non stoichiometry of the film (decreasing with increasing the formation voltage).

The shift in the anodic direction of U_{FB} as a consequence of the anodizing process indicates a decrease of the oxygen vacancy concentration, i.e. an improvement of the oxide stoichiometry, which is so pronounced to cancel the effect of the reduced density of states close to the band edges, suggested by the change in ΔE_{am} and E_U values.

This finding shows how the electronic structure of a Ti–Zr containing mixed oxide is strongly dependent on both the base alloy composition and the forming conditions. This aspect is very important on a practical view point if we take into account that the electronic properties of passive films play a key role in determining the corrosion behaviour of a material by influencing the kinetic of charge exchange at the metal/passive film/electrolyte interface.

5. Conclusions

The band gap value and flat band potential of Ti–Zr containing mixed oxides grown by air exposure and by anodizing ($U_F = 4$ V/SCE) were determined as a function of the film composition by photocurrent spectroscopy. The experimental results showed that E_g^{opt} increases with increasing the Zr content in both air formed and anodic films, in agreement with the theoretical expectation on the base of the described correlation between the band gap values of oxides and the difference of electronegativity of their constituents. The comparison of the experimental results with those predicted by this correlation allowed to evidence an influence on the film structure of the forming conditions and of the Zr/Ti ratio. These last parameters are also important in determining whether the passive films behave like semiconducting or insulating materials.

The photoelectrochemical investigation allowed to get information on the electronic properties of the investigated oxides, which are very important in determining the performances of these materials in different technological fields.

References

[1] Q. Shao, A. Li, W. Zhang, Z. Liu, N. Ming, Chem. Vapor Depos. 12 (2006) 423.
[2] A. Kitiyanan, S. Yoshikawa, Mater. Lett. 59 (2005) 4038.
[3] A. Kitiyanan, S. Ngamsinlapasathian, S. Pavasupree, S. Yoshikawa, J. Solid State Chem. 178 (2005) 1044.
[4] A. Kitiyanan, S. Sakulkhaemaruethai, Y. Suzuki, S. Yoshikawa, Compos. Sci. Technol. 66 (2006) 1259.
[5] J.C. Yu, J. Lin, R.W.M. Kwok, J. Phys. Chem. B 102 (1998) 5094.
[6] M. Hirano, C. Nakahara, K. Ota, O. Tunaike, M. Inagaki, J. Solid State Chem. 170 (2003) 39.
[7] S. Qiu, T.L. Starr, J. Electrochem. Soc. 154 (2007) H472.
[8] B.J. Reddy, B. Chowdhurry, I. Ganesh, E.P. Reddy, T.C. Rojas, A. Fernandez, J. Phys. Chem. B 102 (1998) 10176.
[9] S.Y. Yu, C.W. Brodrick, M.P. Ryan, J.R. Scully, J. Electrochem. Soc. 146 (1999) 4429.
[10] S.Y. Yu, J.R. Scully, C.M. Vitus, J. Electrochem. Soc. 148 (2001) B68.
[11] H. Habazaki, K. Shimizu, S. Nagata, K. Asami, K. Takayama, Y. Oda, P. Skeldon, G.E. Thompson, Electrochim. Acta 48 (2003) 3257.
[12] H. Habazaki, M. Uozumi, H. Konno, K. Shimizu, S. Nagata, K. Asami, K. Matsumoto, K. Takayama, Y. Oda, P. Skeldon, G.E. Thompson, Thin Solid Films 479 (2005) 144.
[13] F. Di Quarto, S. Piazza, M. Santamaria, C. Sunseri, in: H.S. Nalwa (Ed.), Handbook of Thin Film Materials, vol. 2, Academic Press, S. Diego, 2002, p. 373 (Chapter 8).
[14] F. Di Quarto, M. Santamaria, C. Sunseri, Photoelectrochemical techniques in corrosion studies, in: P. Marcus, F. Mansfeld (Eds.), Analytical Methods in Corrosion Science and Technology, Taylor and Francis, Boca Raton, 2006. p. 697 (Chapter 18).
[15] M. Santamaria, D. Huerta, S. Piazza, C. Sunseri, F. Di Quarto, J. Electrochem. Soc. 147 (2000) 1366.
[16] M. Santamaria M, F. Di Quarto, P. Skeldon, G.E. Thompson, J. Electrochem. Soc. 153 (2006) B518.
[17] G.D. Cody, in: J.I. Pankove (Ed.), Semiconductors and Semimetals, vol. 21, Academic Press, London, 1984, p. 11. part B.
[18] D.L. Wood, J. Tauc, Phys. Rev. B 5 (1972) 3144.

[19] M. Santamaria, F. Di Quarto, H. Habazaki, Electrochim. Acta 53 (2008) 2272.
[20] F. Di Quarto, S. Piazza, C. Sunseri, M.C. Romano, J. Phys. Chem. B 101 (1997) 2519.
[21] N.F. Mott, E.A. Davis, Electronic Processes in Non-Crystalline Materials, second ed., Claredon Press, Oxford, 1979.
[22] H. Gerischer, Electrochim. Acta 34 (1989) 1005.
[23] E. McCafferty, J. Electrochem. Soc. 146 (1999) 2863.
[24] S. Piazza, L. Calà, C. Sunseri, F. Di Quarto, Ber. Bunsenges. Phys. Chem. 101 (1997) 932.
[25] P.A. Cox, Transition Metal Oxides, Claredon Press, Oxford, 1992.